International Journal of Nanomedicine

Dovepress
open access to scientific and medical research

Open Access Full Text Article

ORIGINAL RESEARCH

Non-immunogenic dextran-coated superparamagnetic iron oxide nanoparticles: a biocompatible, size-tunable contrast agent for magnetic resonance imaging

Harald Unterweger,[1,*] Christina Janko,[1,*] Marc Schwarz,[2] László Dézsi,[3] Rudolf Urbanics,[4] Jasmin Matuszak,[1] Erik Őrfi,[3] Tamás Fülöp,[3] Tobias Bäuerle,[2] János Szebeni,[3,4] Clément Journé,[5] Aldo R Boccaccini,[6] Christoph Alexiou,[1] Stefan Lyer,[1] Iwona Cicha[1]

[1]Cardiovascular Nanomedicine Unit, Section of Experimental Oncology und Nanomedicine (SEON), Else Kröner-Fresenius-Stiftung-Professorship, ENT Department, University Hospital Erlangen, Friedrich-Alexander-Universitaet Erlangen-Nuernberg, [2]Preclinical Imaging Platform Erlangen (PIPE), Institute of Radiology, University Hospital Erlangen, Erlangen, Germany; [3]Nanomedicine Research and Education Center, Semmelweis University, [4]SeroScience Ltd., Budapest, Hungary; [5]Inserm U1148, Fédération de Recherche en Imagerie Multimodalités (FRIM), X Bichat Hospital, Paris Diderot University, Paris, France; [6]Institute of Biomaterials, Department of Materials Science and Engineering, University Erlangen-Nuremberg, Erlangen, Germany

*These authors contributed equally to this work

Correspondence: Iwona Cicha
Cardiovascular Nanomedicine Unit, Section of Experimental Oncology and Nanomedicine, ENT Department, University Hospital Erlangen, Glückstr 10a, 91054 Erlangen, Germany
Tel +49 9131 854 3953
Fax +49 9131 853 4282
Email iwona.cicha@yahoo.com

Abstract: Iron oxide-based contrast agents have been in clinical use for magnetic resonance imaging (MRI) of lymph nodes, liver, intestines, and the cardiovascular system. Superparamagnetic iron oxide nanoparticles (SPIONs) have high potential as a contrast agent for MRI, but no intravenous iron oxide-containing agents are currently approved for clinical imaging. The aim of our work was to analyze the hemocompatibility and immuno-safety of a new type of dextran-coated SPIONs (SPIONdex) and to characterize these nanoparticles with ultra-high-field MRI. Key parameters related to nanoparticle hemocompatibility and immuno-safety were investigated in vitro and ex vivo. To address concerns associated with hypersensitivity reactions to injectable nanoparticulate agents, we analyzed complement activation-related pseudoallergy (CARPA) upon intravenous administration of SPIONdex in a pig model. Furthermore, the size-tunability of SPIONdex and the effects of size reduction on their biocompatibility were investigated. In vitro, SPIONdex did not induce hemolysis, complement or platelet activation, plasma coagulation, or leukocyte procoagulant activity, and had no relevant effect on endothelial cell viability or endothelial–monocytic cell interactions. Furthermore, SPIONdex did not induce CARPA even upon intravenous administration of 5 mg Fe/kg in pigs. Upon SPIONdex administration in mice, decreased liver signal intensity was observed after 15 minutes and was still detectable 24 h later. In addition, by changing synthesis parameters, a reduction in particle size <30 nm was achieved, without affecting their hemo- and biocompatibility. Our findings suggest that due to their excellent biocompatibility, safety upon intravenous administration and size-tunability, SPIONdex particles may represent a suitable candidate for a new-generation MRI contrast agent.

Keywords: superparamagnetic iron oxide nanoparticles, MRI, hypersensitivity reaction, SPION uptake, hemocompatibility

Introduction

Superparamagnetic iron oxide nanoparticles (SPIONs) and ultra-small superparamagnetic iron oxide nanoparticles (USPIOs) consist of an iron oxide core, which is commonly coated with an organic shell.[1] As contrast agents, SPION/USPIO have been in clinical use for various diagnostic purposes, including magnetic resonance imaging (MRI) of lymph nodes, liver, intestines, and the cardiovascular system.[2,3] Having strong T_2 and T_2* effects in MRI, SPION/USPIO can be detected even at very low concentrations, allowing an increase of MRI sensitivity almost to the cellular level.[4,5] Consequently, SPION-labeling was shown to enable in vivo tracking of mononuclear cells,[6] as well as the real-time visualization of intra-arterial stem cell delivery to target

submit your manuscript | www.dovepress.com
Dovepress
http://dx.doi.org/10.2147/IJN.S138108

regions of the brain.[7] USPIO-enhanced MRI has also been proposed as an excellent tool for precise assessment of blood–brain barrier opening during neurointerventions.[8]

In clinical applications, differences in pharmacokinetics between SPION and USPIO play a major role: due to their smaller hydrodynamic diameter, USPIO are not immediately scavenged by mononuclear phagocytes; therefore, their reported circulation half-life is considerably longer (up to 24 h) as compared with the larger SPIONs (2–4 h),[9] which allows their more widespread distribution in tissues, including atherosclerotic plaques. The USPIO-based contrast agent ferumoxtran (Combidex/Sinerem, dextran-coated particles with a hydrodynamic diameter of 20–40 nm) was extensively utilized to detect and characterize atherosclerotic plaques (reviewed in Tang et al[10]). Multiple studies confirmed the ability of USPIO-enhanced MRI to identify plaque inflammation and vulnerability,[11,12] also within otherwise morphologically "stable" plaques,[13] and in asymptomatic patients.[14] Furthermore, ferumoxtran-enhanced MRI has been shown to predict the expansion and rupture of aortic aneurysms[15] and detect inflammation following ischemic stroke.[16] Importantly, sequential USPIO-enhanced MRI in patients suffering from stenosis of carotid arteries[17] provided evidence that, within 6 months, ferumoxtran particles administered at 2.6 mg Fe/kg were cleared out of the plaque, with no major adverse effects observed following multiple infusions.[17]

In contrast to USPIO, SPIONs are characterized by enhanced liver accumulation, thereby constituting a superb hepatic MRI contrast agent. Low concentrations of SPIONs (0.5 mg Fe/kg of carboxydextran-coated ferucarbotran (Resovist/Ferrixan, 45–60 nm[18–20]), or dextran-coated ferumoxides (Endorem/Feridex),[21] have been used to noninvasively distinguish between benign liver condition (simple steatosis) and nonalcoholic steatohepatitis (NASH), which is highly associated with cardiovascular and renal comorbidities.[22]

Despite promising results in humans, the marketing of intravenous iron oxide-containing contrast agents is currently at a standstill. The production of ferumoxtran was discontinued despite documented diagnostic efficacy and safety.[23] Ferucarbotran and ferumoxides, approved for MRI in the past, were similarly withdrawn from the market. To fulfil the clinical need, the intravenous iron replacement agent ferumoxytol (Feraheme/Rienso, 17–30 nm particles coated with a low-molecular-weight semisynthetic carboxylated polymer) was used as a contrast agent to characterize the myocardial infarct pathology[24,25] and to differentiate simple steatosis from NASH.[26] It must be noted, however, that the required concentrations of ferumoxytol were very high, 4–7.2 mg Fe/kg body weight in myocardial infarct[24,25] and 3.6 mg/kg in patients with liver disease.[26] In the light of the fact that this agent, indicated only for therapy of iron deficiency anemia in patients with chronic renal failure, has, in 2015, received the FDA's strongest type of warning due to the serious risk of potentially fatal anaphylactic reactions upon administration, the use of ferumoxytol for imaging may pose an enormous risk to patients, and underscores the need of a safe iron oxide-based contrast agent.

We have recently described the development of a new type of dextran-coated SPIONs (SPIONdex), which demonstrate superb stability and biocompatibility with endothelial cells.[27] Compared to the previously marketed dextran-coated contrast agent ferumoxides, SPIONdex have several distinct and improved characteristics. Ferumoxides was composed of magnetite nanoparticles with iron concentration 11.2 mg/mL, hydrodynamic diameter 120–150 nm, and zeta potential −13 mV. Those particles were coated with low-molecular-weight (10 kDa) unmodified dextran (9.1 mg/mL), but the formulation also contained mannitol (61.3 mg/mL) and citrate (0.53 mg/mL), which were likely contributors to the negative surface charge, atypical for dextran-coated particles. Moreover, Simberg et al[28] identified – besides the binding of mannan-binding lectins to the dextran coating of ferumoxides – interactions of histidine-rich glycoprotein and kininogen with the iron oxide core, with subsequent binding of the complement lectin and contact clotting factors. These findings indicate that the distribution of dextran molecules on the surface of ferumoxide particles was not sufficiently uniform, with the patchy coating leading to the core exposure that may have contributed to the reported side effects.[29] In contrast, SPIONdex coated with dextran T40 (40 kDa) are characterized by a narrow size distribution (hydrodynamic diameter 80 nm) and nearly neutral charge. Furthermore, the stabilization of the dextran coating by a crosslinking process ensures that the coating is continuous, thus preventing the exposure of the iron core to serum proteins. Following the extensive physicochemical and magnetic characterization of SPIONdex particles,[30,31] we now investigated the key parameters related to their hemocompatibility and immunosafety. To address concerns associated with hypersensitivity reactions to injectable nanoparticulate agents, we tested whether intravenous administration of SPIONdex induces complement activation-related pseudoallergy (CARPA) in pigs. Furthermore, their relaxation properties in T_1-, T_2-, and T_2*-weightings have been investigated to characterize SPIONdex with ultra-high-field MRI. As different diagnostic applications demand the organ- and/or tissue-specific size of

nanoparticles, we additionally investigated the size-tunability of SPIONdex and the effects of size reduction on their overall biocompatibility in vitro.

Methods

Materials and reagents

Cell culture media were purchased from Promo Cell (Heidelberg, Germany). HyClone™ HyQTase™ cell detachment reagent was obtained from GE Healthcare Life Sciences (Linz, Austria) and dispase from Life Technologies GmbH (Logan, UT, USA). Iron (III) chloride hexahydrate, dextranT40 (Mw =40 kDa), and epichlorohydrin were from Sigma Aldrich (Munich, Germany) and iron (II) chloride tetrahydrate was obtained from Merck (Darmstadt, Germany). NaOH, HCl (25%), NH_3 (25%), and nitric acid (65%, w/w) were from Roth (Karlsruhe, Germany). Reagents used for nanoparticle synthesis were of pharmaceutical (Ph. Eur) or highly pure (≥99%) grade.

SPIONdex synthesis and characterization

The tested SPIONs (referred to as SPIONdex in the text) were produced at SEON, University Hospital Erlangen, according to the method described by Unterweger et al.[30] Briefly, co-precipitation of Fe(II) and Fe(III) salts (molar ratio Fe^{3+}/Fe^{2+} =2) in the presence of dextran T40 was performed under argon atmosphere. Following dialysis, the mixture was concentrated using ultrafiltration [molecular-weight cutoff (MWCO) 100 kDa]. To stabilize the coating, epichlorohydrine was added to the NaOH-alkalized SPIONdex suspension in order to induce dextran crosslinking. SPIONdex were subsequently dialyzed, concentrated by ultrafiltration, and sterilized.

In order to examine the size-tunability, the iron concentration during co-precipitation reaction was varied between 70 and 150 mM. The effects of the variation in iron concentration on particle size-tunability were investigated at two different dextran concentrations – 6.9% (w/w) and 11.3% (w/w).

Hydrodynamic diameter and zeta potential of SPIONdex were measured with a Zetasizer Nano ZS (Malvern Instruments, Herrenberg, Germany). Transmission electron microscopy images were taken with a FEI Tecnai 20 microscope (Fei, Hillsboro, OR, USA) and a Gatan US 1000 CCD camera. The magnetization of SPIONdex was measured using a SQUID-based susceptometer QD-MPMS-XL-5, and volume susceptibility was determined with an MS2G magnetic susceptibility system (Bartington, Witney, Oxfordshire, UK). Crystalline phases present in the SPIONdex were determined using X-ray diffraction (Bruker D8 Advance, Billerica, MA, USA). Detailed synthesis description and physicochemical characterization of SPIONdex were reported previously[30,31] and is summarized in the Supplementary materials.

Particle sterility and endotoxin contamination assay

To ensure sterility, determination of microbial contamination via quick agar plate test was performed. Lack of endotoxin contamination was confirmed using the kinetic turbidity Limulus Amebocyte Lysate (LAL) assay, which determines the bacterial endotoxin content, as described in detail in the Supplementary materials.

Blood stability test

The stability of particle suspension in freshly extracted, EDTA-stabilized rabbit whole blood was investigated as described in the Supplementary materials.

Hemocompatibility tests

To assess the hemocompatibility, SPIONdex effects on complement activation, plasma coagulation, as well as platelet aggregation and activation were investigated using freshly drawn whole blood from healthy human volunteers according to the Nanotechnology Characterization Laboratory (NCL, Frederick, MD, USA) protocols. Details of the procedure and the experimental assays are provided in the Supplementary materials. Isolation of human material was approved by the local ethics committee (National Cancer Institute Ethics Office) and written consent was obtained from all donors.

Erythrocyte lysis test

For hemocompatibility testing, lithium–heparin anticoagulated blood was drawn from healthy volunteers and the hemoglobin content in blood was adjusted to 5 mg/mL in phosphate-buffered saline (PBS). Nanoparticles (4, 20, 100, and 500 µg/mL) were incubated with diluted blood for 3 h at 37°C and carefully mixed every 30 min; 1% Triton X-100 and PBS served as positive and negative controls, respectively. The suspension medium (H_2O) of the nanoparticles was tested as vehicle control. To detect the potential interference of nanoparticles with the assay, the positive control was additionally spiked with nanoparticles. As background controls, nanoparticles diluted in H_2O at the respective concentrations were used. After 3 h, erythrocytes were sedimented by centrifugation at 800× *g* for 15 min. The supernatant was centrifuged again for 1.5 h (SPION) or 4 h (USPIO) at 18,000× *g* to sediment nanoparticles. To determine the

content of free hemoglobin, 100 µL supernatant was incubated with 100 µL Drabkin's reagent (Sigma-Aldrich) for 5 min in 96-well plates at 60°C on a heating plate. Drabkin's reagent lyses erythrocytes and converts hemoglobin and its derivatives to methemoglobin and then to cyanmethemoglobin, which was detected by absorption measurement at 590 nm on Microplate Reader Filter Max F5 (Molecular Devices). The use of human blood was approved by the local ethics committee (Klinisches Ethikkomitee des Universitätsklinikums Erlangen) and written informed consent was obtained from all donors.

SPIONdex effect on endothelial cells and leukocytes

The effects of SPIONdex on leukocyte procoagulant activity (PCA), an in vitro indicator of disseminated intravascular coagulation, and on leukocyte proliferation were analyzed using peripheral blood mononuclear cells (PBMCs) isolated from three healthy donors, as described in the Supplementary materials. THP-1 monocytic cell recruitment by TNF-α-stimulated human umbilical vein endothelial cells (HUVECs) under flow conditions, in the presence or absence of SPIONdex, was assessed using bifurcating flow-through cell culture slides (Ibidi®, Munich, Germany) and a programmed peristaltic pump (Ismatec, Wertheim, Germany), as previously reported.[32] The effect of SPIONdex on THP-1 monocytic cell migration was investigated using 96-well Chemo-Tx plates (NeuroProbe, Gaithersburg, MD, USA) and on HUVEC migration, using silicone cell culture inserts (Ibidi, Munich, Germany) and a live-cell imaging microscope, as described in detail in the Supplementary materials. The use of human material was approved by the local ethics committee (Klinisches Ethikkomitee des Universitätsklinikums Erlangen). Written informed consent was obtained from all donors.

Quantification of iron load per cell

To estimate the cellular uptake of nanoparticles, iron concentration per cell was quantified with microwave plasma atomic emission spectroscopy (MP-AES, 4200 device, Agilent). HUVECs (0.5×10^6 cells) and primary human kidney cells (0.25×10^6 cells) seeded in six-well plates were grown until 90% confluence. THP-1-derived macrophages were seeded at 0.25×10^6 and grown for 24 h prior to incubation with nanoparticles. THP-1 monocytes were seeded at 0.5×10^6 cells/mL. Cells were then incubated with medium containing SPIONdex (0–400 µg/mL for suspension cells, adjusted to 0–400 µg/cm^2 for adherent cells) for 24 h, followed by harvesting, washing with medium, and counting. After centrifugation, cell pellets containing a specified number of cells were dissolved in nitric acid for 15 min at 95°C. After the addition of 450 µL water, the emission spectrum of samples was analyzed and compared to the standard curves. SPION-untreated cell samples were used as negative controls, reflecting the baseline cellular iron content in different cell types.

Analysis of complement activation-related pseudoallergy

Studies in a pig model of CARPA were performed according to the protocols established at the Semmelweis University, as previously described by Szebeni.[33] A detailed description of the method is provided in the Supplementary materials.

Briefly, isoflurane-anesthetized Yorkshire pigs (20–25 kg) were administered a bolus injection of the control and test substances (saline, SPIONdex, and zymosan) via the left external jugular vein. Oxygen saturation, $EtCO_2$, respiratory rate, pulmonary arterial blood pressure (PAP), systemic arterial blood pressure (SAP), and heart rate (HR) were continuously monitored. The amount of injected SPIONdex is given as milligrams of Fe per kilogram body weight. Following blood sampling, plasma levels of thromboxane B2 (TXB2, the stable metabolite of TXA2) were quantified using a commercially available ELISA kit (Cayman Chemicals, Ann Arbor, MI, USA). The study protocol was approved by the National Scientific Ethical Committee on Animal Experimentation (ÁTET) and Institutional Animal Welfare Committee of the Semmelweis University (MÁB), Budapest, Hungary.

MRI studies

MRI in a phantom was performed at room temperature with 7 T MRI ClinScan® 70/40 (Bruker BioSpin, Ettlingen, Germany) using a circular polarized 1H mouse whole-body RF coil and corresponding animal bed (Bruker BioSpin).

Table 1 shows the T_1-, T_2-, and T_2*-weighted sequence parameters. Imaging reconstruction parameters (pixel

Table 1 MRI sequence parameters

Relaxation time map	T_1	T_2	T_2*
Sequence	FLASH 3D	Turbo spin echo	Gradient echo
TR (ms)	50	5,000	250
TE (ms)	2.5	8.7, 17.4, 26.1, 34.8, and 43.5	3.19, 7.18, 11.17, 15.16, and 19.15
Flip angle (°)	8 and 42	180	40
Acquisition matrix	192×168	192×168	192×168
Field of view (mm)	34×39	34×39	34×39
Slice thickness (mm)	0.5	0.5	0.5
Acquisition time (min)	5:11	41:59	42:10

Abbreviations: MRI, magnetic resonance imaging; TE, echo time; TR, repetition time.

size: 0.208×0.208 mm^2; Acquisition matrix: 192×168; field of view: 34×39 mm; slice thickness: 0.5 mm) were chosen identically for each sequence.

For measurement, nanoparticle dilutions were molded in 1% agarose within 0.2 mL microcentrifuge tubes (Eppendorf, Hamburg, Germany) to obtain the test concentrations [0, 1:1, 1:1,000, and 1:10,000 SPIONdex (7.57 mg/mL Fe)]. The tubes themselves were embedded in 5% agarose in the mouse bed to reduce vibrations that occurred during the imaging. T_1-, T_2-, and T_2*-weighted MRI was done five times consecutively. Imaging was performed with syngo® MR B15 software. The images were imported into OsiriX (Version 3.8.5) and T1-, T2-, and T2*-maps were drafted out of the images. Regions of interest (ROI) were chosen manually within the samples and exported to Microsoft® Excel.

In order to test the correlations between relaxation times and SPION concentration, the 0.2 mL microcentrifuge tubes were filled with particles at 0, 2, 4, 6, 8, and 10 µg/mL Fe in 1% agarose gel. Subsequently, the tubes were embedded in 5% agarose gel. The prepared samples were measured in MRI as described earlier.

In vivo pilot study with SPIONdex particles was carried out on two wild-type mice. MRI examinations were performed with 7T Pharmascan (Bruker BioSpin), using the quadrature volume coil (40 mm inner diameter) and a model 1025 monitoring and gating system from SA Instruments. The sequence was a T_2-weighted image with the following parameters: 15 axial slices with slice thickness 1 mm, echo time: 36.47 ms, repetition time: 1,747 ms, number of excitations: 5, rapid acquisition with relaxation factor: 8. The matrix size was 512×512. The animals were anesthetized with isofluorane (3%–4% for induction and 1%–2% for maintenance) and their body temperature was maintained at 37°C. The SPIONdex (2.6 mg iron/kg bw), diluted in saline to 100 µL volume, were administered intravenously via retroorbital injection. MRI scans were performed before the administration, within 15 min post-administration, and at 1, 3, and 24 h post-administration, and the signal intensity of the liver was observed. The animals were sacrificed 26 h post-injection, and the organs isolated for histological analysis as described in the Supplementary materials. The study was performed at the Fédération de Recherche en Imagerie Multimodalités (FRIM), France, with permission from the local ethics committee for animal experimentation at Inserm (Comité d'éthique 121 Paris Nord). The study was carried out in compliance with European Directive 2010/63/CE on the protection of animals used for scientific purposes and according to institutional standards for humane treatment of animals.

Statistical analyses

Unless stated otherwise, the data are expressed as mean ± SEM. The comparison between untreated and SPIONdex-treated in vitro samples was done using Student's *t*-test, Signed Rank test, or ANOVA on Ranks. For MRI measurements, mean, SD, and coefficient of variance (CV) were calculated for each test sample. Two-sided, unpaired Student's *t*-test was used to compare relaxation times of each SPIONdex concentration and the agarose control. Changes in hemodynamic and hematological parameters versus pre-injection baseline values were analyzed using one-way ANOVA with Dunnett's post hoc comparisons. $P<0.05$ was considered statistically significant.

Results

Physicochemical characteristics

An extensive physicochemical characterization of SPIONdex nanoparticles has been previously published by Unterweger et al[30,31] (see also Supplementary materials). Briefly, SPIONdex (core size 4.3±0.9 nm), had a hydrodynamic diameter of 79.6±0.6 nm in water and zeta potential −3.2 mV.

Sterility

To confirm the lack of microbial contamination, quick agar sterility tests (Figure S1), as well as the kinetic turbidity LAL assays for the presence of endotoxin, were performed, showing that SPIONdex were free of bacterial contamination (Figures S1 and S2), with endotoxin levels <0.105 EU/mL.

Blood stability ex vivo

The blood stability of SPIONdex was evaluated using EDTA-anticoagulated rabbit whole blood (Figure S3). SPIONdex particles were stable and exhibited neither macro- nor microscopically detectable aggregates over the whole observation period (60 min). As the detection limit of the microscope used is ~200 nm, it can be concluded that no aggregates ≥200 nm had formed upon the contact of SPIONdex with whole blood.

Hemocompatibility

To assess the hemocompatibility of SPIONdex particles, their effects on erythrocytes, plasma coagulation, platelet aggregation and activation, as well as complement activation, were investigated. Incubation of blood with SPIONdex did not cause any erythrocyte damage and release of hemoglobin (Figure 1A).

As shown in Figure 1B, plasma incubation with SPIONdex had no effect on prothrombin time (extrinsic

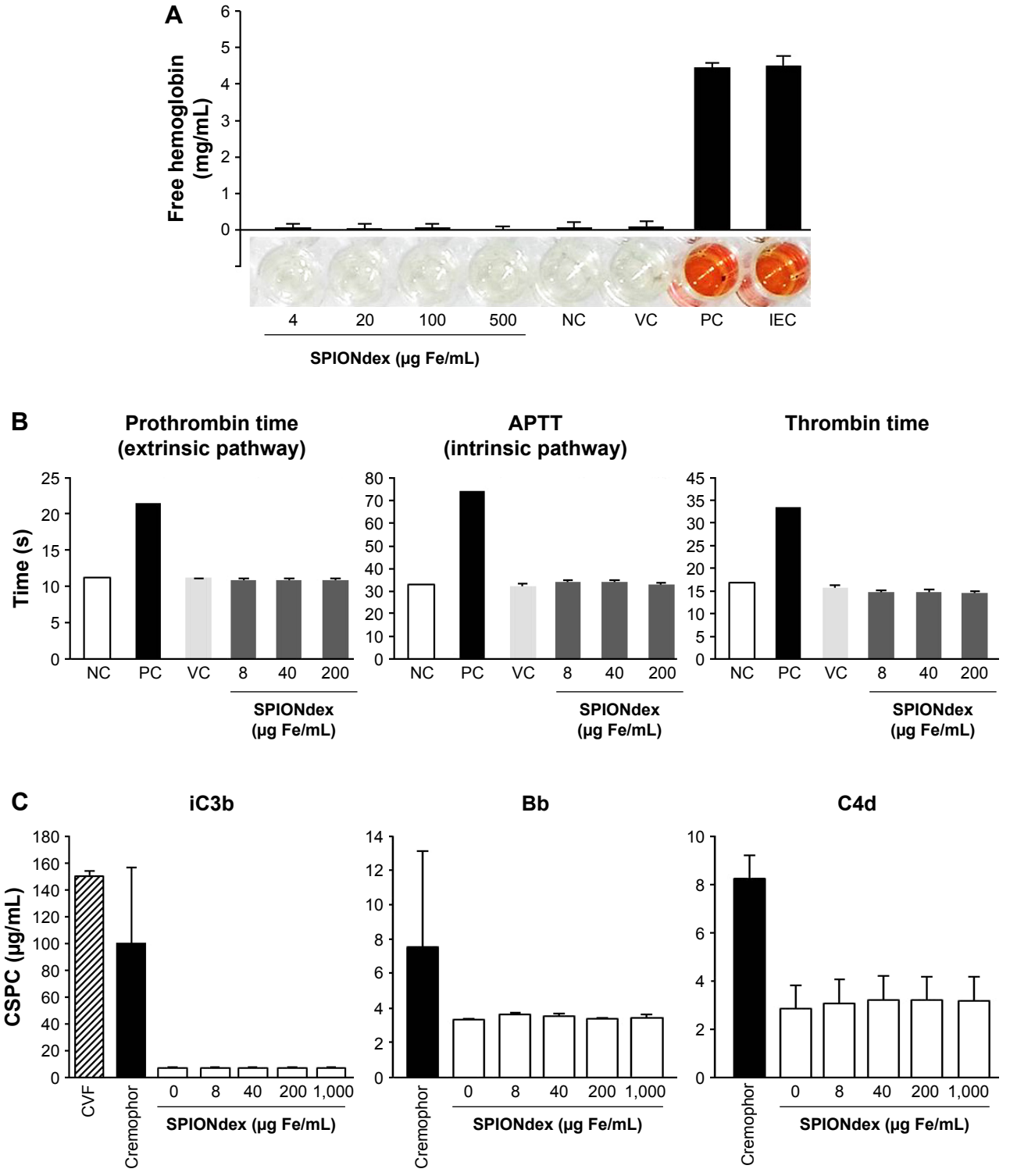

Figure 1 Hemocompatibility of SPIONdex.

Notes: (**A**) Erythrocyte lysis: erythrocyte lysis test of SPIONdex. Free hemoglobin in supernatant serves as marker for damage of erythrocytes. The experiment was performed with the blood of three healthy donors in triplicates. The controls used were: NC (erythrocytes in PBS); VC (erythrocytes in PBS + H_2O); PC (erythrocytes in PBS + 1% Triton X-100); inhibition/enhancement control (PC + SPIONdex). (**B**) Coagulation time: Platelet poor human plasma was treated with SPIONdex for 30 min, followed by adding the respective coagulation activation reagent to each sample (Neoplastine for prothrombin time, $CaCl_2$ for APTT, and thrombin for thrombin time) and subsequently coagulation time was measured. (**C**) Complement activation: human plasma was incubated with SPIONdex, followed by analysis of complement split products: iC3b component of complement, Bb component of complement for alternative activation pathway, and C4d component of complement for classical activation pathway. CVF and Cremophor served as positive controls. Mean ± standard deviation of replicate samples of plasma pooled from three donors are shown.

Abbreviations: APTT, activated partial thromboplastin time; ATP, adenosine triphosphate; CSPC, complement split product component; CVF, cobra venom factor; IEC, inhibition/enhancement control; Fe, iron; NC, negative control; PBS, phosphate-buffered saline; PC, positive control; SPIONdex, dextran-coated superparamagnetic iron oxide nanoparticles; VC, vehicle control.

pathway), activated partial thromboplastin time (APTT, intrinsic pathway), and did not affect the thrombin time.

In unstimulated samples, treatment with SPIONdex had no effect on platelet aggregation or ATP release (Figure S4, upper panel). However, it must be noted that, at the highest tested concentration (200 µg/mL), an interference with the light-scattering-based measurement was observed as resulting from the presence of SPIONs. SPIONdex did not affect the collagen-stimulated platelet aggregation and activity (Figure S4, bottom panel).

SPIONdex did not induce complement activation in vitro up to a concentration of 1 mg/mL. Neither classical nor alternative activation pathways were affected by the presence of SPIONdex particles (Figure 1C).

Intravenous injections of nanoparticles have been linked to fatal coagulopathy in mice,[34,35] resulting from phosphatidyl serine–tissue factor complex presentation on the surface of leukocytes (leukocyte PCA). As shown in Figure S5, no effect of SPIONdex on PCA was detectable up to a concentration of 320 µg/mL.

We have subsequently investigated the effects of SPIONdex on leukocyte proliferation. Upon 72-h incubation, SPIONdex (20–500 µg/mL) had a minor influence on unstimulated leukocyte proliferation (Figure 2A). Interestingly, in phytohemagglutinin (PHA)-activated cells, a dose-dependent inhibition of leukocyte proliferation was observed at higher doses of SPIONdex particles (100 and 500 µg/mL), indicative of a slight immunosuppressive effect (Figure 2B).

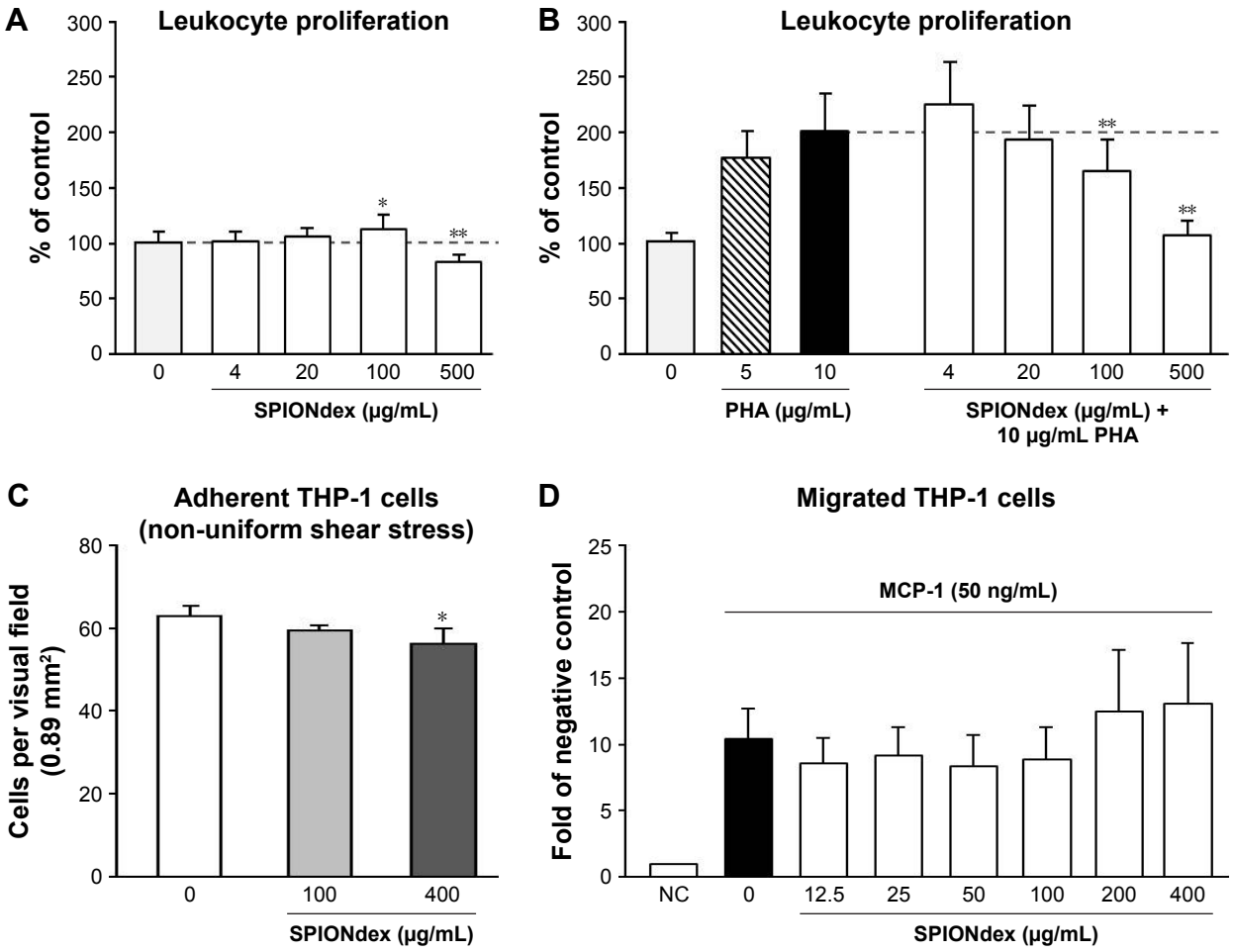

Figure 2 Effects of SPIONdex on white blood cells.

Notes: (**A**) Unstimulated leukocytes were incubated for 72 h with SPIONdex. (**B**) Leukocyte proliferation was stimulated with PHA in the presence or absence of SPIONdex. Cell proliferation is expressed as a percentage of untreated control. Mean ± SD of replicate samples of leukocytes pooled from three donors are shown. (**C**) HUVECs were exposed to non-uniform shear stress for 18 h, followed by stimulation with TNF-α for 2 h, and perfusion with THP-1 monocytic cells. The graph shows numbers of firmly adherent cells (mean ± SEM of three independent experiments). (**D**) THP-1 monocytic cells were incubated with SPIONdex for 2 h under constant stirring, followed by 1 h chemotaxis to MCP-1 using a modified Boyden chamber assay. Data are expressed as fold of NC (mean ± SEM of four independent experiments). *$P<0.05$, **$P<0.01$.

Abbreviations: HUVECs, human umbilical vein endothelial cells; MCP-1, monocyte chemoattractant protein-1; NC, negative control; PHA, phytohemagglutinin; SD, standard deviation; SEM, standard error of the mean; SPIONdex, dextran-coated superparamagnetic iron oxide nanoparticles; THP-1, a human monocytic cell line; TNF-α, tumor necrosis factor-alpha.

Effects on vascular cell function

Lack of SPIONdex effects on endothelial cell viability was previously confirmed in static cultures and under physiologic-like flow.[36] (Figure S6). In the flow-based monocyte adhesion assay, no major effects of SPIONdex on the TNF-α-induced monocytic cell recruitment by HUVECs were observed (Figure 2C). Solely upon treatment with 400 µg/mL of SPIONdex, slightly reduced numbers of adherent monocytic cells were detected in regions of non-uniform shear stress.

Concerning monocytic cell chemotaxis, SPIONdex particles induced a slight biphasic effect: Between 12.5 and 100 µg/mL, the numbers of transmigrated THP-1 monocytic cells were decreased by 20%, and a slight increase in monocytic chemotaxis to monocyte chemoattractant protein-1 (MCP-1) was detected at 200–400 µg/mL of SPIONdex; however, these changes were not statistically significant (Figure 2D).

Nanoparticle internalization by cells

To investigate whether SPIONdex biocompatibility/bio-inertness results from their low cellular uptake by non-phagocytic cells, primary HUVECs, human kidney cells, and THP-1 monocytic cells, as well as THP-1-derived macrophages were incubated with SPIONdex particles for 24 h, followed by washing and the measurement of cellular iron content with MP-AES. The internalization of SPIONdex was very low in HUVECs and THP-1 monocytic cells (Figure 3), as well as in human kidney cells (Figure S7) upon 24 h incubation. As shown in Figure 3, a statistically significant uptake was observed only at the two highest tested concentrations, although the measured iron concentration did not exceed 0.3 pg/cell for HUVECs (SPIONdex at 400 µg/cm^2) and 0.15 pg/cell for THP-1 cells (SPIONdex at 400 µg/mL). In contrast, a strong dose-dependent increase in particle uptake was detected in THP-derived macrophages. After 24 h incubation, the concentration of cellular iron was ~5 pg/cell in cells treated with 50 µg/cm^2 and >15 pg/cell in macrophages treated with 400 µg/cm^2 SPIONdex.

No CARPA reaction to SPIONdex infusion

SPIONdex at two different doses (0.5 and 5 mg Fe/kg) was intravenously administered in domestic pigs, in order to assess the potential cardiovascular changes resulting from hypersensitivity reactions. The control and test substances were injected as a bolus in the external jugular vein, starting with the negative control injection (5 mL saline). After the subsequent injection of SPIONdex at 0.5 mg/kg, no cardiovascular, blood cell, or skin changes [except slight pulmonary arterial blood pressure (PAP) elevation at 10 and 15 min] were observed (Figure 4A). In order to detect tachyphylaxis (desensitization), a 5× higher dose of particles was administered 30 min later. As no CARPA reaction was observed after this bolus injection of 5 mg/kg of SPIONdex, the presence of full tachyphylaxis was concluded. Zymosan at 0.1 mg/kg (positive control) resulted in a dramatic increase of PAP. In the subsequent animal, the reaction to 10× higher dose was tested, whereby no CARPA was observed upon the injection of SPIONdex at 5 mg/kg (Figure S8A). Full tachyphylaxis was confirmed by the injection of a 2× higher dose 30 min later, which also caused no reaction. Zymosan, administered as above at 0.1 mg/kg, caused a strong CARPA reaction (Figure S8B).

After the first 0.5 mg/kg SPIONdex injection, thromboxane B2 (TXB2) measurement in blood samples showed a slight TXB2 increase during the early phase (1 min; Figure 4B). Upon subsequent administration of a 10× higher dose, a slightly stronger TXB2 elevation at 1 min followed

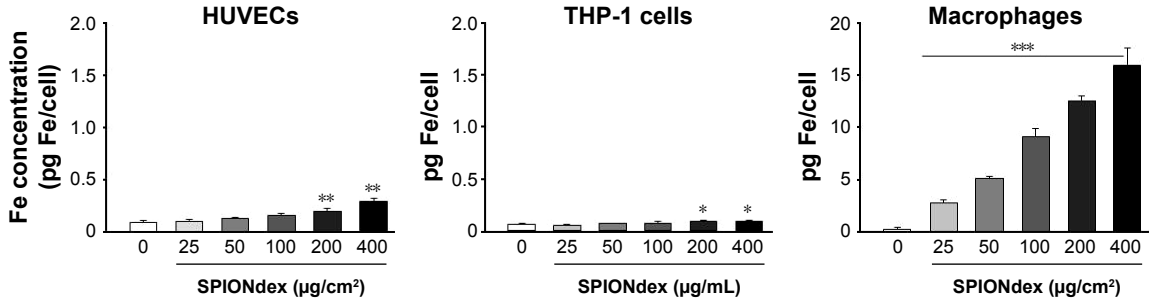

Figure 3 Internalization of SPIONdex by cells.

Notes: Cells were incubated with SPIONdex as indicated. Iron content was measured in cell pellets containing specified number of cells. Note the *y*-axis scale differences for HUVECs and THP-1 cells versus macrophages. *$P<0.05$, **$P<0.01$, and ***$P<0.001$ vs unstimulated control.

Abbreviations: Fe, iron; HUVECs, human umbilical vein endothelial cells; THP-1, a human monocytic cell line; SPIONdex, dextran-coated superparamagnetic iron oxide nanoparticles.

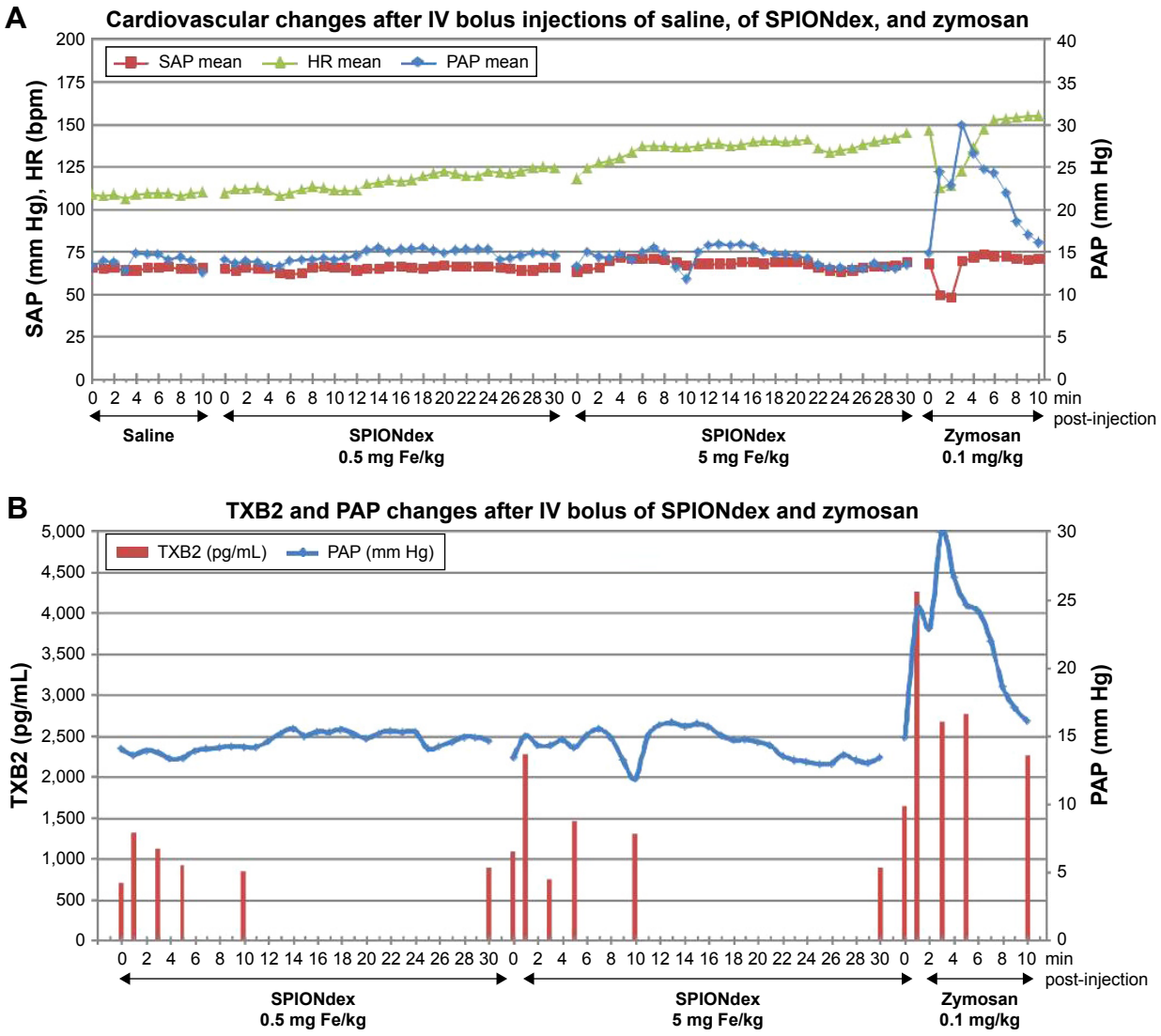

Figure 4 Cardiovascular reaction to SPIONdex in a pig model of CARPA.
Notes: (**A**) Saline and SPIONdex (0.5 mg Fe/kg), followed by 5 mg/kg SPIONdex and zymosan IV bolus injections. PAP, SAP, and HR were continuously monitored for up to 30 min. (**B**) TXB2 plasma concentrations in relation to PAP changes upon administration of SPIONdex (0.5 mg Fe/kg), followed by 5 mg/kg SPIONdex and 0.1 mg/kg zymosan. Mean values of two independent experiments are shown.
Abbreviations: CARPA, complement activation-related pseudoallergy; Fe, iron; HR, heart rate; IV, intravenous; PAP, pulmonary arterial blood pressure; SAP, systemic arterial blood pressure; SPIONdex, dextran-coated superparamagnetic iron oxide nanoparticles; TXB2, thromboxane B2.

by decrease at 3 min was observed. Zymosan administration evoked a strong TXB2 increase, which persisted for 10 min (Figure 4B).

MRI in phantom

To characterize SPIONdex particles using MRI, relaxation times of different concentrations of SPIONdex in agarose gel (0, 1:10,000, and 1:1,000 solutions of SPIONdex; stock: 7.57 mg Fe/mL) were determined. As shown in Figure 5, the T_1-, T_2-, and T_2*-relaxation times decreased with increasing SPIONdex concentrations, and significant differences were recorded when compared to controls (1% agarose; Figure 5A–D).

For determining the precision of the MRI quantification, the coefficient of variance in the ROIs (CV) of the measurements (quadruple assessment) was calculated. Mean CVs were <1% for T_1-relaxation times, 4.8% for T_2-relaxation times, and 9.6% for T_2*-relaxation times. The maximum relative standard deviations were <11% ($CV_{T1\text{-}time}$ =0.8%; $CV_{T2\text{-}time}$ =5.7%; $CV_{T2^*\text{-}time}$ =10.5%). Corresponding values are shown in Figure 5 and Table 2.

In vivo MRI

In vivo pilot imaging with SPIONdex particles was performed in wild-type mice. As shown in Figure 6A, a strong decrease in T_2-weighted liver signal intensity was detected directly upon

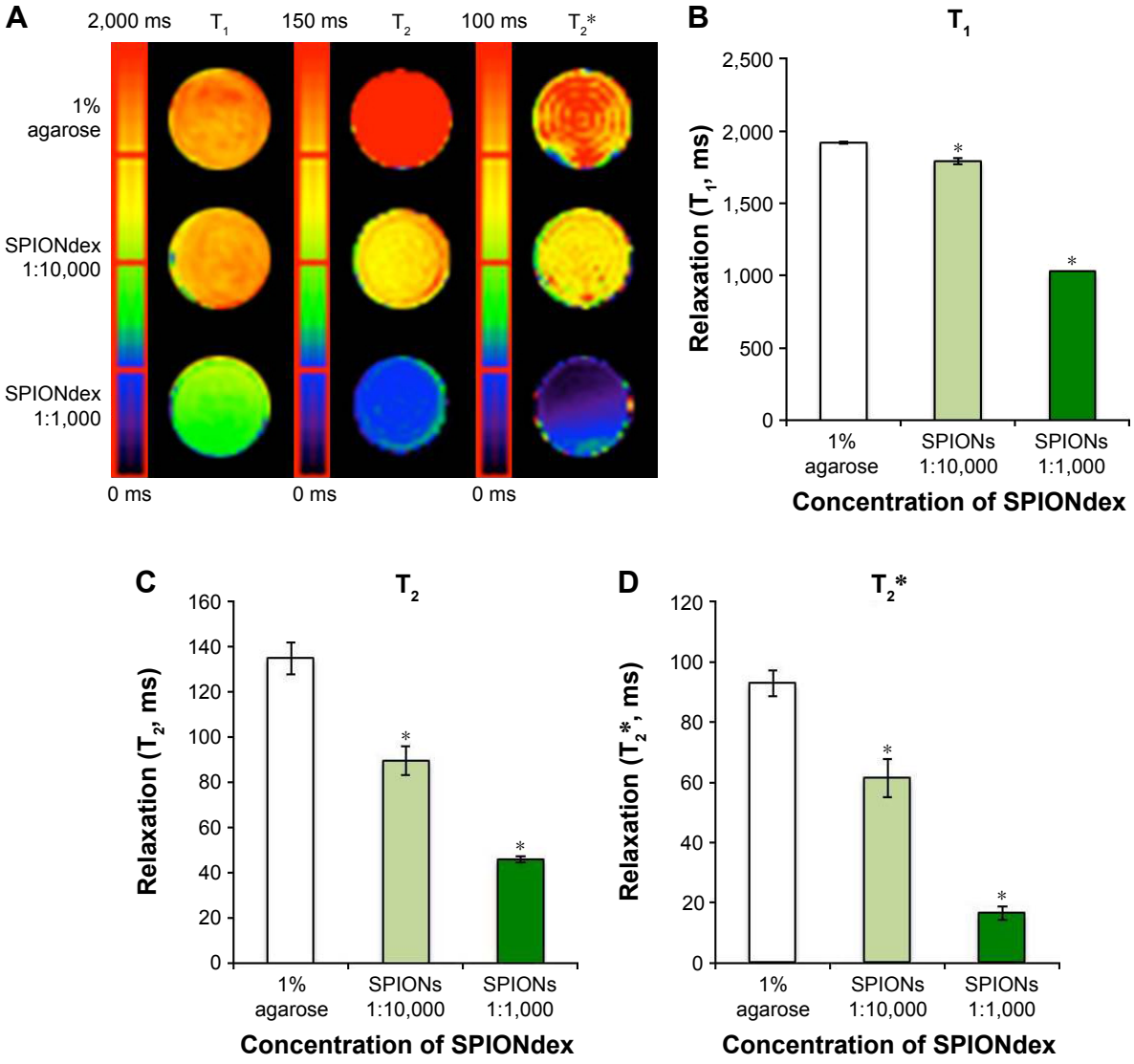

Figure 5 Relaxation times of SPIONdex concentration series. The 0.2 mL microcentrifuge tubes were filled with 0, 1:10,000, and 1:1,000 SPIONdex (7.57 mg Fe/mL stock solution) in 1% agarose gel and embedded in 5% agarose gel.

Notes: (**A**) Color-coded maps of agarose-embedded SPIONdex show reduced T_1-, T_2-, and T_2*-times with the increasing iron content. Diameter of the vials shown =8 mm. (**B**) T_1-, (**C**) T_2- and (**D**) T_2*-relaxation times. Data are expressed as mean ± standard deviation of quadruple measurements. *$P<0.05$ vs agarose control.

Abbreviations: Fe, iron; SPIONdex, dextran-coated superparamagnetic iron oxide nanoparticles.

the intravenous administration of SPIONdex in mice. The effect remained observable for 24 h post-administration, indicating the potential of SPIONdex as an MRI contrast agent for liver imaging. The presence of SPIONdex in the liver of test animals was subsequently confirmed on histological sections by Prussian blue staining (Figure 6B).

Table 2 List of all measured relaxations times

	T_1-relaxation times (ms)	T_2-relaxation times (ms)	T_2*-relaxation times (ms)
Agarose	1,918.5±4.7	135.0±7.7	93.3±2.8
SPIONdex 1:10,000	1,791.3±15.1	89.8±4.9	61.8±3.8
SPIONdex 1:1,000	1,029.0±5.8	45.8±1.5	16.8±2.1

Note: Data are expressed as mean ± standard deviation of quadruple measurements.

Abbreviation: SPIONdex, dextran-coated superparamagnetic iron oxide nanoparticles.

Size-tuning and biocompatibility of ultrasmall iron oxide nanoparticles

Size-tuning of the particles was achieved by variation of the iron concentration during the coprecipitation reaction. As shown in Figure 7, the hydrodynamic size of the nanoparticles increased with increasing iron concentration. This effect was more pronounced when the dextran concentration was decreased in parallel. At high dextran concentrations (11.3%, w/w; Figure 7A), the hydrodynamic particle size could be tuned between 17.0 and 44.0 nm at iron concentrations in the range between 70 and 150 mM, respectively. Interestingly, at lower dextran concentrations (6.9%, w/w; Figure 7B), much broader size range (between 25.1 and 129.1 nm) was achieved at the same iron concentration range.

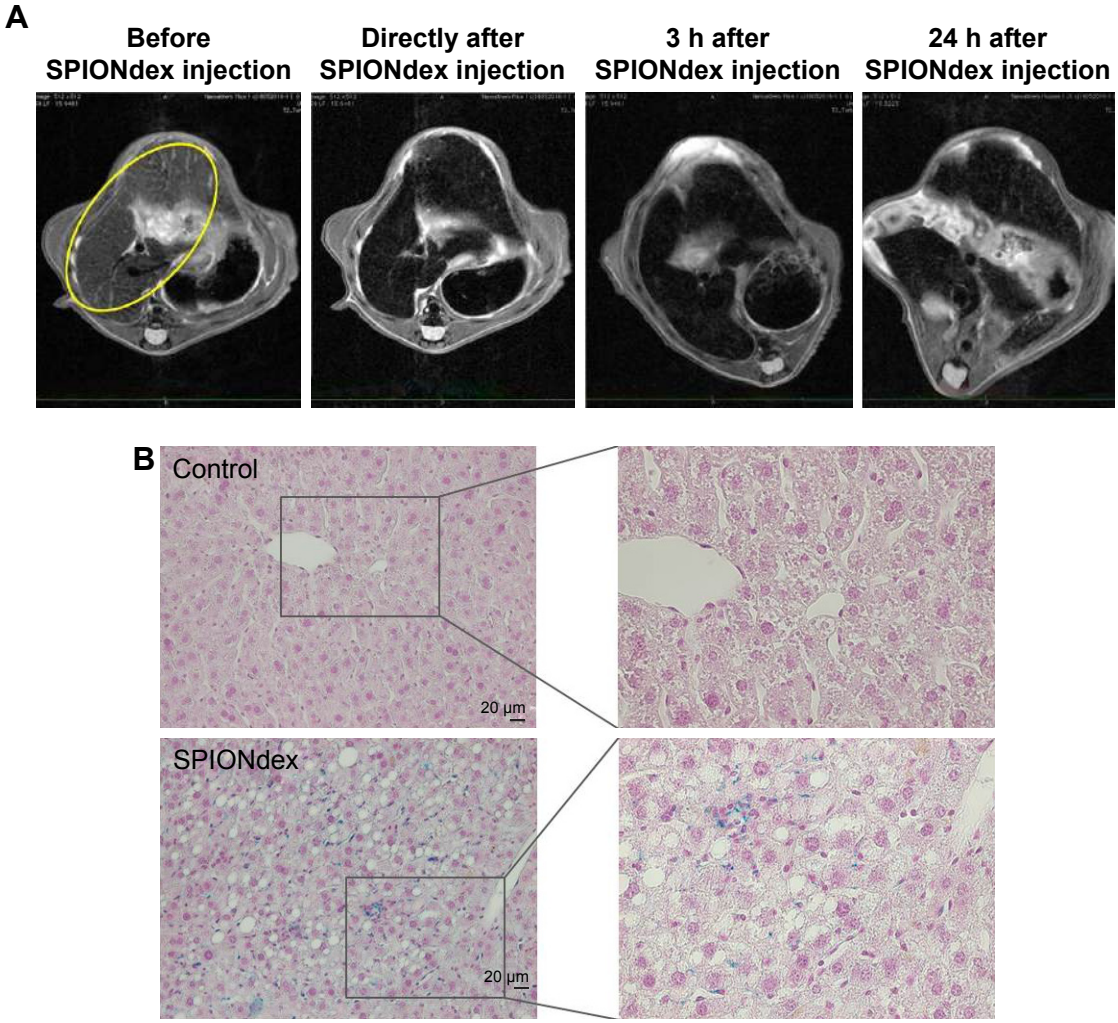

Figure 6 Contrast-enhanced MRI with SPIONdex in vivo. SPIONdex (2.6 mg iron/kg bodyweight) were administered intravenously via retroorbital injection.
Notes: (**A**) The representative T2-weighted hepatic MRI images before the administration, within 15 min post-administration, and at 3 and 24 h post-administration (liver is indicated by the yellow ellipse). Signal intensity decreases in the liver directly after the injection, and the hyposignal remained observable 24 h after SPIONdex injection. (**B**) Histological analysis. Iron accumulation in liver at 26 h post-administration was detected using Prussian blue stain. Representative images at ×20 magnification (left panel) or ×40 magnification (right panel) are shown.
Abbreviations: MRI, magnetic resonance imaging; SPIONdex, dextran-coated superparamagnetic iron oxide nanoparticles.

As shown in Figure 7C and D, decreasing the hydrodynamic diameter also slightly reduced the magnetic susceptibility of the produced particles. The respective TEM images of larger (SPION) and smaller (USPIO) dextran-coated particles are shown in Figure 7E and F.

In order to investigate whether a considerable reduction in particle hydrodynamic diameter affects hemo- and biocompatibility, tests on ultra-small superparamagnetic iron oxide nanoparticles (USPIOdex, <30 nm) were performed according to the same protocols as described for SPIONdex particles. As shown in Figure 8, incubation of USPIOdex with blood caused neither nanoparticle aggregation (Figure 8A), nor erythrocyte damage and release of hemoglobin (Figure 8B). Plasma coagulation parameters were not affected by USPIOdex (Figure 8C), and no effects on endothelial cell viability were detected upon prolonged incubation with these particles up to the highest tested concentration (400 µg Fe/mL) using real-time cell analysis (Figure 8D) or live-cell imaging (data not shown).

Discussion

Apart from considerable research interest, there is a growing clinical need to apply iron oxide nanoparticles for signal detection of infection and inflammation, as well as for the in vivo cell tracking. SPION-enhanced MRI was shown to be effective in the noninvasive evaluation of the severity of NASH and differentiation of NASH patients from patients with simple steatosis. Clinical studies indicated that imaging of atherosclerosis using USPIO-enhanced MRI harbors tremendous diagnostic and prognostic potential, both in asymptomatic population, as well as in subjects at risk of future or recurrent cardiovascular events. However, the

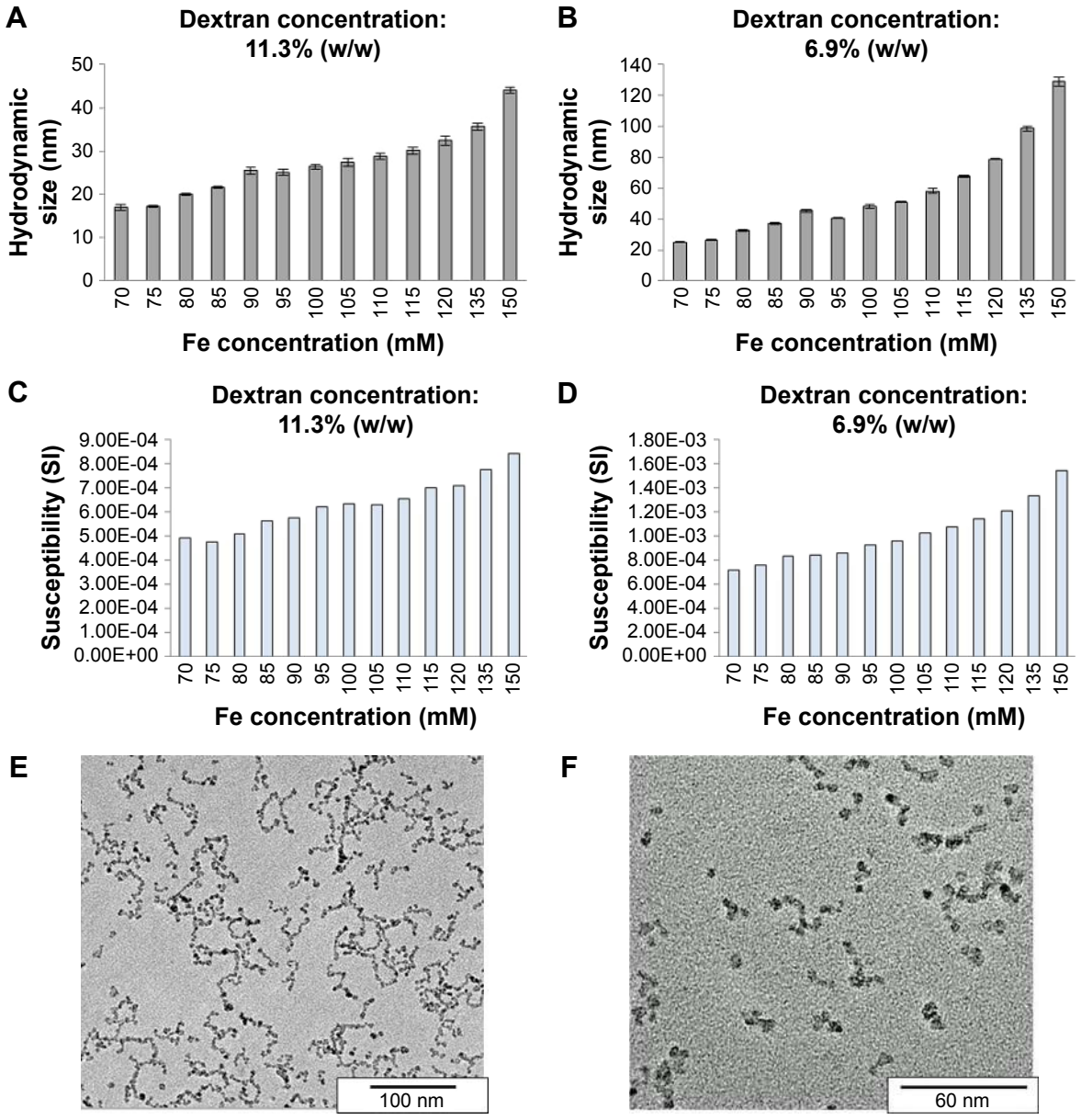

Figure 7 Hydrodynamic size and corresponding volume susceptibility of dextran-coated iron oxide nanoparticles, in dependence of the iron concentration during coprecipitation.

Notes: (**A** and **B**) Fe concentration during coprecipitation reaction was varied between 70 and 150 mM at two different dextran concentrations: 11.3% (w/w) and 6.9% (w/w). (**C** and **D**) The volume susceptibility is a dimensionless parameter, which can be determined in the SI or cgs unit system. The presented values are given in the SI unit system. TEM images of (**E**) larger and (**F**) smaller particles are shown.

Abbreviations: cgs, centimeter-gram-second; Fe, iron; SI, international system of units; TEM, transmission electron microscopy.

withdrawal of iron oxide-based contrast agents from the market has halted further studies that would broadly validate their clinical utility in larger cohorts.

The nephrotoxicity related to gadolinium-based contrast agents (GBCA) remains a concern. Although not acutely toxic, certain gadolinium chelates represent a risk in patients with impaired renal function due to gadolinium retention in liver, spleen, heart, skin, kidneys, and bladder, which can lead to nephrogenic systemic fibrosis. The accumulation of gadolinium deposits in hepatocytes and Kupffer cells may also exclude the possibility of sequential or repeated liver scans. Additionally, the exposure of patients with impaired renal function to 0.27–0.68 mmol/kg of linear GBCA was associated with cerebral accumulation of gadolinium, triggering transient signs of neurological disorders.[37] Following the FDA recommendation that GBCA use should be restricted to medical conditions that demand additional information provided by this contrast agent and that repetitive GBCA imaging should be avoided, the Pharmacovigilance and Risk Assessment Committee of the European Medicines Agency has recommended

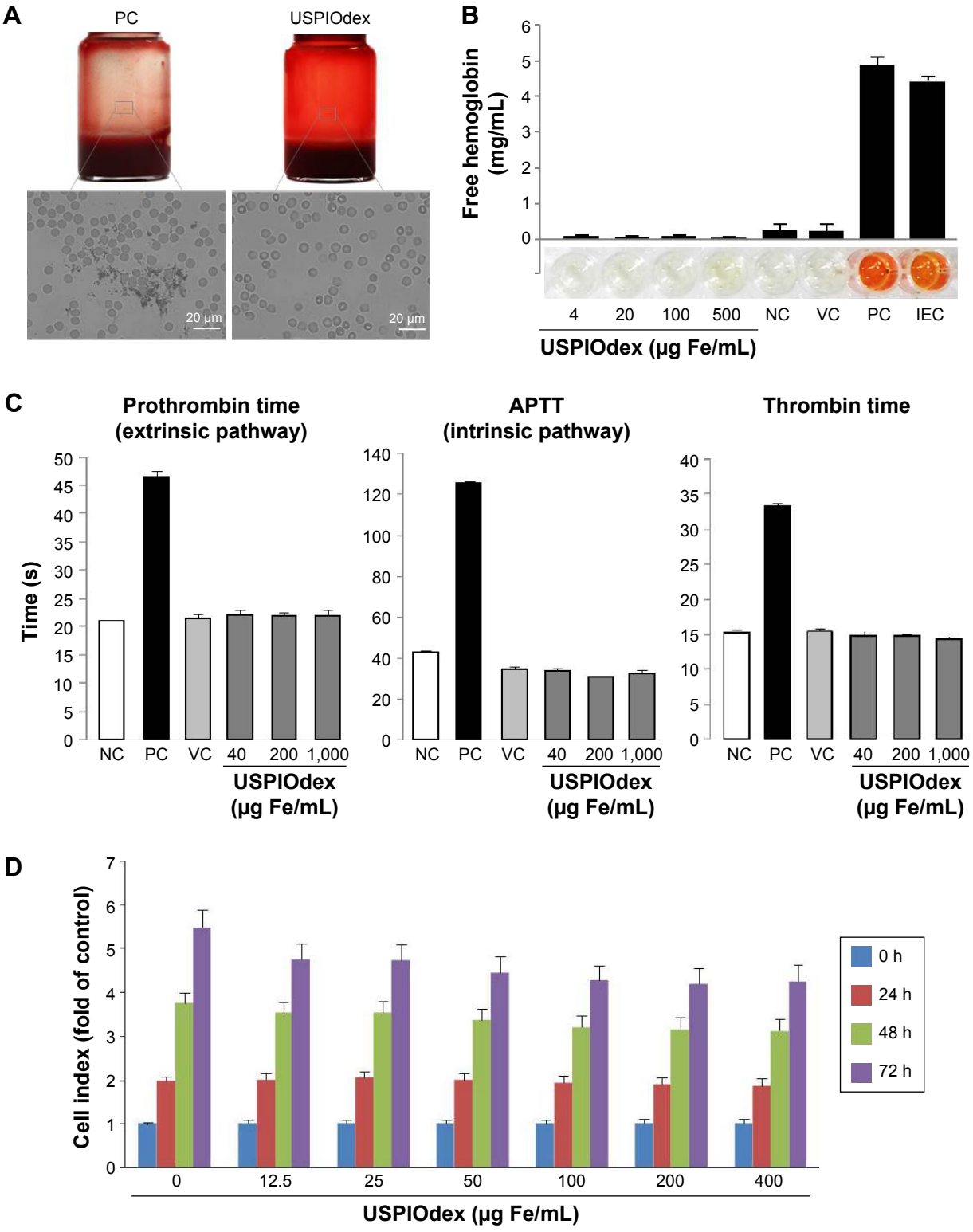

Figure 8 Hemo- and biocompatibility of ultra-small dextran-coated iron oxide nanoparticles.

Notes: (**A**) Investigation on the blood stability of USPIOdex in EDTA-anticoagulated rabbit whole blood. Blood sample was mixed with USPIOdex to an iron concentration of 1 mg/mL. Microscopic images were taken after 45 min of incubation. PC: lauric acid-coated SPIONs. (**B**) Erythrocyte lysis: erythrocyte lysis test of USPIOdex. Free hemoglobin in supernatant serves as marker for damage of erythrocytes. NC: erythrocytes in PBS; VC: erythrocytes in PBS + H_2O; PC: erythrocytes in PBS + 1%Triton X-100; IEC (PC + USPIOdex). (**C**) Coagulation time: platelet poor human plasma was treated with USPIOdex for 30 minutes, followed by adding the respective coagulation activation reagent to each sample (Neoplastine for prothrombin time, $CaCl_2$ for APTT, and thrombin for thrombin time) and subsequent coagulation time measurement. (**D**) USPIOdex effects on ECs viability was investigated using real-time cell analysis (xCELLigence system). HUVECs were seeded at 2×10^3 cells per well. At 24 h after seeding, medium containing USPIOdex was added to the wells. Cell growth was monitored every 10 min for 72 h.

Abbreviations: APTT, activated partial thromboplastin time; ECs, endothelial cells; EDTA, ethylenediaminetetraacetic acid; Fe, iron; IEC, inhibition/enhancement control; NC, negative control; PBS, phosphate-buffered saline; PC, positive control; USPIOdex, dextran-coated ultra-small superparamagnetic iron oxide nanopareticles; VC, vehicle control.

the suspension of marketing authorizations for four linear intravenous GBCA in March 2017. A new generation of iron oxide-based contrast agents with superior safety profile, that could be administered in patients diagnosed with cardiovascular and nonalcoholic fatty liver disease, independent of their renal function is, therefore, urgently needed.

Depending on their size and coating, SPION/USPIO-based contrast agents may circulate for extended periods of time and, upon intravenous infusion, may induce undesired effects. To address this issue, we performed extensive studies, demonstrating that SPIONdex did not induce complement or platelet activation in vitro, had no effect on coagulation or leukocyte PCA and did not affect unstimulated leukocyte proliferation. Solely in activated leukocytes, a dose-dependent inhibition of leukocyte proliferation was observed at high doses of SPIONdex (>100 μg/mL). In line with this, a slight suppression of monocytic cell recruitment by TNF-α-stimulated endothelial cells exposed to high doses of SPIONdex (400 μg/mL) was detected in non-uniform shear stress region, indicative of a weak anti-inflammatory effect of these particles. Altogether, the SPIONdex particles showed superb blood stability and in vitro hemocompatibility, which suggests a favorable safety profile for potential in vivo application. Of importance, furthermore, is their low internalization by non-phagocytic cells. This is in line with the colloid-stabilizing function of dense dextran coating, which prevents particle agglomeration on one hand and, on the other hand, renders them neutrally charged. HUVECs and other non-phagocytic cells lacking carbohydrate scavenger receptors are expected to internalize dextran-coated SPIONs only to a minimal degree, mainly via clathrin-mediated endocytosis. Interestingly, previous studies showed that avid internalization of dextran-coated SPIONs (feumoxides, ferumoxtran-10) by macrophages occurs via SR-A1 and is largely independent of C-type lectin receptors scavenging dextrans.[38] Concerning the cellular fate of SPIONs, their clearance via normal metabolism involving ferritin and by cell division was previously demonstrated. The ferritin pathway is, moreover, the most common mechanism of iron metabolism upon in vivo therapeutic administration.[39,40] Our data indicate that the clearance of these particles from ECs is rapid and independent of particle size. As shown in Figure S9, the incubation of ECs with SPION/USPIOdex for 24 h resulted in 2.5 to 3-fold increase in cell iron content, which returned to untreated control levels within 48 h post-incubation, indicating a fast degradation of these particles.

There are several risks related to intravenous administration of iron oxide-based nanosystems, the most serious of them being the hypersensitivity reactions. Apart from potential life-threatening cardiopulmonary distress, such hypersensitivity to intravenous contrast agents may preclude their multiple or sequential applications.[33] This is underscored by recent safety concerns regarding the use of ferumoxytol, the administration of which was associated with multiple cases of anaphylactoid (hypersensitivity) reactions. In ~75% of all cases (79, 18 of which fatal), the reaction began during the infusion or within 5 min after administration, and >50% experienced anaphylactic reactions with a repeated dose of ferumoxytol. It is estimated that ~2%–10% of patients will react to intravenous drugs with mild-to-severe hypersensitivity reaction.[33] In order to evaluate the risk of SPIONdex particles as a trigger of hypersensitivity, we performed the dedicated CARPA tests in a pig model.[41] It was previously shown that pigs are extremely sensitive to infused nanoformulations, including liposomal doxorubicin (Doxil®). Interestingly, independent of the physicochemical characteristics of the trigger particles (eg, material, size, charge), the pattern of induced cardiopulmonary responses is essentially the same.[33] Our present studies showed that the intravenous bolus administration of undiluted SPIONdex particles did not induce CARPA in pigs, neither at 0.5 nor at 5 mg/kg.

In the pilot in vivo MRI studies, we furthermore demonstrated the ability of SPIONdex to serve as potential contrast agent that causes a significant change in relaxation times at low concentrations (0.03 mmol Fe/L), as compared to the concentrations of GBCA that are generally used for MRI examinations (eg, Gadovist, 0.05–0.2 mmol/kg bodyweight). Additionally, by changing the synthesis parameters, we achieved the size reduction of dextran-coated particles down to 20–30 nm (USPIOdex). Importantly, this radical reduction in size did not have any deleterious effect on the particle hemo- and biocompatibility, as demonstrated in multiple in vitro and ex vivo assays. SPIONdex size can, thus, be tuned without affecting their exceptional biocompatibility, which underscores their potential for organ/application-dependent adaptation.

Our findings suggest that, due to their superb safety profile, low immunogenicity, and size-tunability, SPIONdex/USPIOdex particles represent a suitable candidate for new-generation MRI contrast agents, offering the possibility of sequential imaging at a low risk of hypersensitivity reactions. The presented pilot studies in vivo represent a major step toward GMP-compliant development of these particles for the clinical MRI applications. However, the acceptance of the clinical radiologists will be decisive in order to validate the diagnostic and prognostic value of new iron oxide-based

contrast agents in clinical trials and ensure their broader and more efficient implementation in standard practice.

Acknowledgments

This work was supported by the European Union ("Nano-Athero" project FP7-NMP-2012-LARGE-6-309820), the Deutsche Forschungsgemeinschaft [German Research Foundation] (CI 162/2-1 and AL 552/8-1), the Bavarian State Ministry of the Environment and Consumer Protection, the Bundesministerium für Bildung und Forschung [Federal Ministry of Education and Research] (grant 01DM14004), and the Cluster of Excellence Engineering of Advanced Materials. The authors thank Doctor MA Dobrovolskaia and Professor SE McNeil (Nanotechnology Characterization Lab, Frederick National Laboratory for Cancer Research, Frederick, MD 21702, USA) for help in conducting relevant experiments. The excellent technical support from TM Potter, BW Neun, A Dongargaonkar, J Rodriguez (all from the Nanotechnology Characterization Lab) is gratefully acknowledged. Further, the authors thank Jonas Granzow from Preclinical Imaging Platform Erlangen for help with MRI measurements in phantoms, Eveline Schreiber from the Section of Experimental Oncology and Nanomedicine for performing the MP-AES measurements, and Doctor Jan Zaloga for critical revision of the manuscript. S Lyer and I Cicha are equally contributing senior authors.

Disclosure

János Szebeni is employed by SeroScience Ltd. The authors report no conflicts of interest in this work.

References

1. Laurent S, Saei AA, Behzadi S, Panahifar A, Mahmoudi M. Superparamagnetic iron oxide nanoparticles for delivery of therapeutic agents: opportunities and challenges. *Expert Opin Drug Deliv*. 2014;11(9):1449–1470.
2. Wang YX, Hussain SM, Krestin GP. Superparamagnetic iron oxide contrast agents: physicochemical characteristics and applications in MR imaging. *Eur Radiol*. 2001;11(11):2319–2331.
3. Chavhan GB, Babyn PS, Thomas B, Shroff MM, Haacke EM. Principles, techniques, and applications of T2*-based MR imaging and its special applications. *Radiographics*. 2009;29(5):1433–1449.
4. Bulte JW, Kraitchman DL. Monitoring cell therapy using iron oxide MR contrast agents. *Curr Pharm Biotechnol*. 2004;5(6):567–584.
5. Diwoky C, Liebmann D, Neumayer B, et al. Positive contrast of SPIO-labeled cells by off-resonant reconstruction of 3D radial half-echo bSSFP. *NMR Biomed*. 2015;28(1):79–88.
6. Richards JM, Shaw CA, Lang NN, et al. In vivo mononuclear cell tracking using superparamagnetic particles of iron oxide: feasibility and safety in humans. *Circ Cardiovasc Imaging*. 2012;5(4):509–517.
7. Walczak P, Wojtkiewicz J, Nowakowski A, et al. Real-time MRI for precise and predictable intra-arterial stem cell delivery to the central nervous system. *J Cereb Blood Flow Metab*. Epub 2016 Jan 1: 271678X16665853.
8. Janowski M, Walczak P, Pearl MS. Predicting and optimizing the territory of blood-brain barrier opening by superselective intra-arterial cerebral infusion under dynamic susceptibility contrast MRI guidance. *J Cereb Blood Flow Metab*. 2016;36(3):569–575.
9. Elias A, Tsourkas A. Imaging circulating cells and lymphoid tissues with iron oxide nanoparticles. *Hematology Am Soc Hematol Educ Program*. 2009;1:720–726.
10. Tang TY, Muller KH, Graves MJ, et al. Iron oxide particles for atheroma imaging. *Arterioscler Thromb Vasc Biol*. 2009;29(7):1001–1008.
11. Kooi ME, Cappendijk VC, Cleutjens KB, et al. Accumulation of ultrasmall superparamagnetic particles of iron oxide in human atherosclerotic plaques can be detected by in vivo magnetic resonance imaging. *Circulation*. 2003;107(19):2453–2458.
12. Trivedi RA, Mallawarachi C, U-King-Im JM, et al. Identifying inflamed carotid plaques using in vivo USPIO-enhanced MR imaging to label plaque macrophages. *Arterioscler Thromb Vasc Biol*. 2006;26(7):1601–1606.
13. Howarth SP, Tang TY, Trivedi R, et al. Utility of USPIO-enhanced MR imaging to identify inflammation and the fibrous cap: a comparison of symptomatic and asymptomatic individuals. *Eur J Radiol*. 2009;70(3):555–560.
14. Degnan AJ, Patterson AJ, Tang TY, Howarth SP, Gillard JH. Evaluation of ultrasmall superparamagnetic iron oxide-enhanced MRI of carotid atherosclerosis to assess risk of cerebrovascular and cardiovascular events: follow-up of the ATHEROMA trial. *Cerebrovasc Dis*. 2012;34(2):169–173.
15. Richards JM, Semple SI, MacGillivray TJ, et al. Abdominal aortic aneurysm growth predicted by uptake of ultrasmall superparamagnetic particles of iron oxide: a pilot study. *Circ Cardiovasc Imaging*. 2011;4(3):274–281.
16. Saleh A, Schroeter M, Ringelstein A, et al. Iron oxide particle-enhanced MRI suggests variability of brain inflammation at early stages after ischemic stroke. *Stroke*. 2007;38(10):2733–2737.
17. Sadat U, Howarth SP, Usman A, Tang TY, Graves MJ, Gillard JH. Sequential imaging of asymptomatic carotid atheroma using ultrasmall superparamagnetic iron oxide-enhanced magnetic resonance imaging: a feasibility study. *J Stroke Cerebrovasc Dis*. 2013;22(8):e271–e276.
18. Tomita K, Tanimoto A, Irie R, et al. Evaluating the severity of non-alcoholic steatohepatitis with superparamagnetic iron oxide-enhanced magnetic resonance imaging. *J Magn Reson Imaging*. 2008;28(6):1444–1450.
19. Asanuma T, Ono M, Kubota K, et al. Super paramagnetic iron oxide MRI shows defective Kupffer cell uptake function in non-alcoholic fatty liver disease. *Gut*. 2010;59(2):258–266.
20. Tonan T, Fujimoto K, Qayyum A, et al. CD14 expression and Kupffer cell dysfunction in non-alcoholic steatohepatitis: superparamagnetic iron oxide-magnetic resonance image and pathologic correlation. *J GastroenterolHepatol*. 2012;27(4):789–796.
21. Tanimoto A, Yuasa Y, Shinmoto H, et al. Superparamagnetic iron oxide-mediated hepatic signal intensity change in patients with and without cirrhosis: pulse sequence effects and Kupffer cell function. *Radiology*. 2002;222(3):661–666.
22. Malhi H, Allen AM, Watt KD. Nonalcoholic fatty liver: optimizing pretransplant selection and posttransplant care to maximize survival. *Curr Opin Organ Transplant*. 2016;21(2):99–106.
23. Bernd H, De Kerviler E, Gaillard S, Bonnemain B. Safety and tolerability of ultrasmall superparamagnetic iron oxide contrast agent: comprehensive analysis of a clinical development program. *Invest Radiol*. 2009;44(6):336–342.
24. Yilmaz A, Dengler MA, van der Kuip H, et al. Imaging of myocardial infarction using ultrasmall superparamagnetic iron oxide nanoparticles: a human study using a multi-parametric cardiovascular magnetic resonance imaging approach. *Eur Heart J*. 2013;34(6):462–475.
25. Alam SR, Shah AS, Richards J, et al. Ultrasmall superparamagnetic particles of iron oxide in patients with acute myocardial infarction: early clinical experience. *Circ Cardiovasc Imaging*. 2012;5(5):559–565.

26. Smits LP, Coolen BF, Panno MD, et al. Noninvasive differentiation between hepatic steatosis and steatohepatitis with MR imaging enhanced with USPIOs in patients with nonalcoholic fatty liver disease: a proof-of-concept study. *Radiology*. 2016;278(3):782–791.
27. Matuszak J, Dorfler P, Zaloga J, et al. Shell matters: Magnetic targeting of SPIONs and in vitro effects on endothelial and monocytic cell function. *Clin Hemorheol Microcirc*. 2015;61(2):259–277.
28. Simberg D, Park JH, Karmali PP, et al. Differential proteomics analysis of the surface heterogeneity of dextran iron oxide nanoparticles and the implications for their in vivo clearance. *Biomaterials*. 2009; 30(23–24):3926–3933.
29. Kurata T, Tanimoto A, Shinmoto H, Yuasa Y, Kuribayashi S. Questionnaire survey of acute and delayed adverse reactions to ferumoxides. *Radiat Med*. 2005;23(7):468–473.
30. Unterweger H, Tietze R, Janko C, et al. Development and characterization of magnetic iron oxide nanoparticles with a cisplatin-bearing polymer coating for targeted drug delivery. *Int J Nanomedicine*. 2014; 9:3659–3676.
31. Unterweger H, Subatzus D, Tietze R, et al. Hypericin-bearing magnetic iron oxide nanoparticles for selective drug delivery in photodynamic therapy. *Int J Nanomedicine*. 2015;10:6985–6996.
32. Cicha I, Regler M, Urschel K, Goppelt-Struebe M, Daniel WG, Garlichs CD. Resveratrol inhibits monocytic cell chemotaxis to MCP-1 and prevents spontaneous endothelial cell migration through Rho kinase-dependent mechanism. *J Atheroscler Thromb*. 2011;18(12): 1031–1042.
33. Szebeni J. Complement activation-related pseudoallergy: a stress reaction in blood triggered by nanomedicines and biologicals. *Mol Immunol*. 2014;61(2):163–173.
34. Greish K, Thiagarajan G, Herd H, et al. Size and surface charge significantly influence the toxicity of silica and dendritic nanoparticles. *Nanotoxicology*. 2012;6(7):713–723.
35. Nabeshi H, Yoshikawa T, Matsuyama K, et al. Amorphous nanosilicas induce consumptive coagulopathy after systemic exposure. *Nanotechnology*. 2012;23(4):045101.
36. Matuszak J, Baumgartner J, Zaloga J, et al. Nanoparticles for intravascular applications: physicochemical characterization and cytotoxicity testing. *Nanomedicine (Lond)*. 2016;11(6):597–616.
37. Barbieri S, Schroeder C, Froehlich JM, Pasch A, Thoeny HC. High signal intensity in dentate nucleus and globus pallidus on unenhanced T1-weighted MR images in three patients with impaired renal function and vascular calcification. *Contrast Media Mol Imaging*. 2016;11(3): 245–250.
38. Chao Y, Karmali PP, Simberg D. Role of carbohydrate receptors in the macrophage uptake of dextran-coated iron oxide nanoparticles. *Adv Exp Med Biol*. 2012;733:115–123.
39. Iancu TC. Ultrastructural pathology of iron overload. *Baillieres Clin Haematol*. 1989;2(2):475–495.
40. Caperna TJ, Failla ML, Steele NC, Richards MP. Accumulation and metabolism of iron-dextran by hepatocytes, Kupffer cells and endothelial cells in the neonatal pig liver. *J Nutr*. 1987;117(2):312–320.
41. Szebeni J, Bedőcs P, Csukás D, Rosivall L, Bunger R, Urbanics R. A porcine model of complement-mediated infusion reactions to drug carrier nanosystems and other medicines. *Adv Drug Deliv Rev*. 2012; 64(15):1706–1716.